Water Resour Manage (2010) 24:2703–2720
DOI 10.1007/s11269-009-9575-2

Geospatial Rainfall Modelling at Eastern Nepalese Highland from Ground Environmental Data

Nazzareno Diodato · Gianni Tartari · Gianni Bellocchi

Received: 3 October 2009 / Accepted: 27 December 2009 /
Published online: 19 January 2010

Abstract The study presents a geospatial knowledge transfer framework by accommodating precipitation maps for the Eastern Nepalese Highland (ENH) across an area of about 100,000 km^2. For this remote area, precipitation–elevation relationships are not homogeneously distributed, but present a chaotic gradient of correlations at altitude ranges. This is mainly due to impervious orography, extreme climate, and data scarcity (most of the rain gauges in Himalaya are located at valley bottoms). Applying geostatistical models (e.g. multivariate geospatial approaches) is difficult in these zones. This makes the ENH an interesting test area where we obtained monthly precipitation spatial patterns for a 30-year period (1961–1990). The aim was to both capture orographic meso-α spatial regimen ($\sim$30 km) and local pattern variability ($\sim$10 km). Data from 58 FAO raingauges were used plus data from an atmospheric weather station (AWS Pyramid) operating at 5,050 m a.s.l., used to compensate the gap of precipitation pattern presents in the area surrounding the Mount Everest. In these complex orographically remote areas of the Himalayas, monsoon precipitation systems exhibit important topographical interactions and spatial correlations, depending on the scale at which the primary variable (e.g., precipitation) and co-variables (e.g., elevation) are recorded and analysed. Precipitations were assessed for months—May, July and September—representative

N. Diodato (✉) · G. Bellocchi
Met European Research Observatory, GEWEX Network—World Climate Research Programme, via Monte Pino, 82100 Benevento, Italy
e-mail: scodalabdiodato@gmail.com

G. Tartari
Ev-K2-CNR Committee, 24126 Bergamo, Italy

G. Tartari
Water Research Institute (IRSA), National Research Council (CNR), 20047 Brugherio, Milan, Italy

of the monsoon season. For the rainiest month (July), cokriging indicated a range of precipitation values from ∼100 mm over the Tibetan Plateau to ∼500 mm in the southern part of Nepal, up to ∼900 mm towards the pre-Himalayan range. For July, cokriging precipitation map also showed correspondence with the map of vegetation pattern, and therein lies the clue to using multivariate geostatistical models as flexible approaches for estimating precipitation spatial patterns in remote areas.

Keywords Cokriging · Digital Elevation Model (DEM) · Highland · Nepal · Rainfall

1 Introduction

> Sky and Earth, above and below, acting in mutual resonance.
> When the moon is approaching from above, the mountains give off steam from below, and incorporated *chhi* come together and unite. This is the spontaneous *Tao* of Nature. (...)
> Rain, dew and frost, everything comes from Earth, and not descended from sky.
> Wang Chhung, 83 AD (from Needham J., 1986. Science and Civilisation in China, Einaudi ed., p. 569).

Precipitation is as an important climatic variable affecting water resources, hydrological forcing and vegetation growing. Today, geospatial statistical approaches in Geographical Information Systems (GIS) are also welcomed to supply ecological attributes in the form of spatial data for use in a variety of applications and models (e.g. Bindlish and Barros 2000; Goovaerts 2000; Diodato 2005; Attorre et al. 2007; Vicente-Serrano et al. 2007; Pons and Ninyerola 2008; Mirás-Avalos et al. 2009). Despite the great importance of climate inputs to their analyses, many users do not have a substantial background in geospatial climatology (the study of the spatial patterns of climate) and are, therefore, not in a position to critically assess the suitability of spatial climate data sets for a particular application (Daly 2006). The recent availability of high-resolution surface climate data sets at the continental-to-global scale offers good opportunity for discussion of the suitability of spatial climate data sets. Incorporating modelling into the GIS allows local deviation from regional patterns to be identified and to make available results from mapping as part of the geographical audit and for development of environmental indicators (Aspinall and Pearson 2000; Jain et al. 2001). This is particularly true for remote mountainous areas such as the Nepalese region, where the topographical complexity, ungauged areas and detection problems make difficult climatic maps construction. The variegated morphology of this region, made of plains, mountainous groups and highlands, has in fact important consequences on atmospheric circulation exacerbating the climate spatial variability processes, which determine a non-uniform and unpredictable distribution of weather and precipitation types and a large spectrum of associated hydrogeomorphological events (Dahal et al. 2006). The bands of maximum precipitation in such situations are variable, and depend on factors such as the process of blocking and uplifting of moisture-bearing winds amplifying precipitation on windward slopes, and can sharply decrease it on leeward slopes downwind (Smith 1979; Daly et al. 1994, 2002). For this reason, rainfall-related spatial pattern models of various complexity and nature may be required for different regions in order to account for geographical complexity. This has led to efforts to estimate high resolution precipitation spatial data over Himalayan Asia related to remote sensing, according to Tropical Rainfall Measurement Mission (TRMM) at 5×5 km resolution (Bookhagen and Burbank 2006), satellite radar data experiment (Anders et al. 2006), and numerical simulation approaches such as EA-clim at 5×5 km resolution derived from MRI/JMA 20-km-mesh AGCM (Yatagai et al. 2005). However, in a recent inter-comparison, Bhowmik and Das (2007) highlighted the limitations of coarse resolution standard climate products, which are derived from remote sensing observations, suggesting that there is a need for higher resolution analysis with adequate raingauge observations to retain important aspects of the summer monsoon. For instance, evaluating the TRMM precipitation pattern with ground based measurements is difficult, due to the general lack of raingauges in the Nepalese region (Anders et al. 2006). Studies at sub-basin scale provided instead useful insights into local variability and precipitation-generating processes (e.g., Barros and Lang 2003). It is however difficult upscaling from this research to generalize about wider spatial patterns, especially across mountainous relieves. On the other hand, the extrapolation from a raingauge network for mapping precipitation via a statistical algorithm (such as the PRISM method of Daly et al. 2002) relies on complex relationships between precipitation and topography which are difficult to justify given the sparse sampling of gauge networks and space–time variability of weather conditions. Thus, among the techniques of interpolation that use ground raingauges, geostatistical approach provides an attractive alternative to extract the maximum of spatial information for defining spatial patterns of precipitation in mountainous regions.

Current knowledge about annual and seasonal precipitation patterns around Nepalese region is derived from rain gauges, and regionalization studies are available (e.g., Leemans and Cramer 1991; Singh and Singh 1996; Shrestha 2000; Yin et al. 2008). However, detailed analyses of the spatial variability of Nepalese areas still need to be done (Basistha et al. 2008). An approach taking into account the impact of topography on precipitation was developed by Zhou et al. (2005) to raise the accuracy of precipitation interpolation within Yangtze River basin (southern China). Seasonal and annual distributions of rainfall in the Chenab basin (western Himalaya) were studied by Arora et al. (2006) using kriging approach. With the advent of remote sensing techniques, the processes controlling precipitation distribution are detected at finer scale (5–20 km), though the number of satellite measurements of monthly or seasonal rainfall amounts is significantly lower than that of ground-based gauges (Bookhagen and Burbank 2006). Remotely sensed storm events and monsoon rains revealed, however, large gradients in seasonal precipitation totals over small ($\sim$10 km) spatial scales, not linearly related to elevation (Barros and Lang 2003; Lang and Barros 2004; Anders et al. 2006; Yatagai and Kawamoto 2008). This makes difficult applying multivariate geostatistical surface station-based approaches, such as cokriging extension. In such respect, the Eastern Nepalese Highland (ENH) target area of this study (26–29° latitude North, 86–89° longitude East) is an interesting trial test. Spatial statistics models have the advantage of covering long temporal span and trends for assessing ground precipitation estimates and uncertainty by extracting all information available from rain gauges. A reliable precipitation mapping approach based on a limited number of gauge-data is desirable for mountainous areas, provided that the data are subject to different kinds of errors, including local disturbances to flow and the difficulty of measuring rainfall in mountainous terrains (Diodato 2005).

In this study, we developed a rainfall geospatial modelling for mapping monthly precipitation spatial patterns for the ENH region over a 30-year climate period (1961–1990). The geospatial model was supported by multivariate geostatistical approach with the purpose to capture both orographic meso-α spatial regime (~30 km) and local pattern variability (~10 km), using data from 59 raingauges over an area placed between 86–89° longitude East and 26–29° latitude North. The technique of cokriging was chosen conditioned on both rain gauges data, to search for sub-regional climatic settings (e.g., atmospheric flux direction within anisotropic gradients), and auxiliary elevation data, to search for local orographic influences (e.g., a more reliable precipitation–terrain interaction within detrending and shifting effects). As temporal test, monsoon precipitation maps for May, July and September were generated at scale of ~10 km, compatible with remarkable variations on spatial patterns observed in the Nepalese region (Anders et al. 2006).

2 Materials and Methods

2.1 Description of the Study Area and Datasets

The most eastern part of Nepal (and neighbour areas in India and Tibetan region of China) is a topographically complex region of the Asian south-east (Fig. 1a), with an extension of approximately 100,000 km^2 (Fig. 1b, c), placed north-east of the Ganges river basin. The region ranges from the southern plain and foothills areas, which provide groundwater resources for irrigation and drinking as well as for industrial purposes, to middle mountain river-valleys, with elevation ranging from 1,000 to 3,000 m, and successive high mountains (3,000–5,000 m) and Tibetan Plateau, with elevation above 5,000 m (Fig. 1c).

The southern plain areas are subtropical. The middle mountains are instead subtropical in valley bottoms but warm temperate on valley sides and cool temperate on higher ridges, which experience occasional snowfall. The high Himalayan mountains are alpine with a frigid climate above the snowline (Kansakar et al. 2004). This area lies south of the high Himalayan range connecting Lobuche area with AWS Pyramid

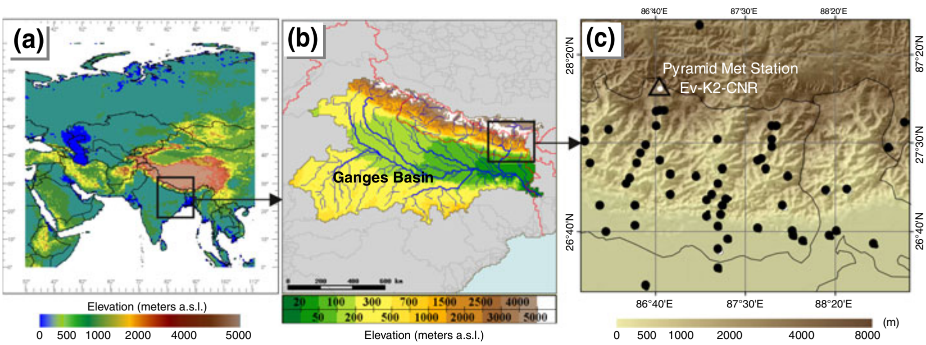

Fig. 1 Location of the study area (**a**), Ganges river basin (**b**) and eastern Nepal's sub-region (ENH) with point-raingauges overlaided to orographic hillshade (**c**)

(5,050 m) and Mount Everest (8,848 m) at the northeastern border of the Sagarmatha National Park, Nepal.

Extrapolation of the relationship snow–rainfall–elevation indicates that snow and rain are equally distributed at about 2,000 m, and all the precipitation occurs as snow above 5,050 m (Singh 1997). However, it is well-known that precipitation throughout the Ganges basin, as well as overall the Nepal region, is highly concentrated in monsoon period between late spring and early autumn (May–October). In such respect, two representative sites can be described for the climate of ENH (Fig. 2): a large monsoon period from May to October, for rainy mountainous areas with abundant vegetation (Fig. 2a), and a longer and drier winter, interrupted by summery precipitation, for highlands over 4,000 m (Fig. 2b). On both cases however, even when winter precipitation comes on time, the planted wheat crop cannot give a sufficient yield as the soils dry down very fast before the crop matures (e.g., March) unless irrigation is provided (Sharma 1979).

After the floods of 1954 and 1955 over northern India, the Meteorological Department was again requested by the Central Water Commission to install, between 1955 and 1958, about 120 raingauges in the Himalayas, including Nepal. With the establishment of Nepal's Meteorological Department in Katmandu, the entire network of stations was taken over by the department in 1962, strengthening it in recent years to about 264 stations with data being available for about 10–40 years (Dhar and Nandargi 2005). In this area, operates since 1989 the Ev-K2-CNR Committee, a research unit of the Italian Research National Council (CNR, http://www.evk2cnr.org/cms), in collaboration with the Nepal Academy of Science and Technology (NAST, http://www.nast.org.np). At the Pyramid Laboratory Observatory, placed at 27.95° North and 86.80° East, and 5,050 m a.s.l. is operating an atmospheric weather station (AWS Pyramid) used to compensate the gap of precipitation pattern presents in the area surrounding the Mount Everest. The raingauge data used in this study correspond to the averages of the monthly precipitation data from 1961 to 1990 recorded in 58 stations derived from LocClim–FAO Database (Grieser et al. 2006), plus the AWS Pyramid Database (Bertolani et al. 2000) that registered data in the most recent period 1994–2000. In total, 59 raingauges were used. Monthly totals (aggregated up from daily totals) were averaged across all available years to characterize long-term precipitation regimes. Only 34% of the above stations were incomplete, their series resulting reduced to 22–28 years. However, differences in record lengths between stations should not influence results meaningfully, as verified also by variography.

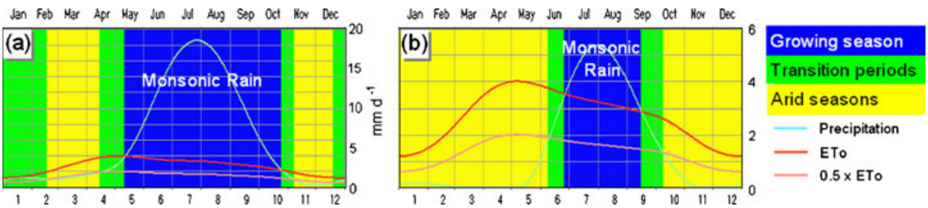

Fig. 2 Climograms of eastern Nepal for (**a**) vegetated mid-elevation mountainous areas, and (**b**) unvegetated high-elevation area of Sagarmatha National Park, near to AWS Pyramid. Season vegetation pattern is also illustrated with coloured bands (arranged by New LocClim-FAO Software (Grieser et al. 2006))

All the spatial elaborations were carried out by using Geostatistical and Spatial Analyst modules implemented in ArcGIS 9.0–ESRI software (Johnston et al. 2001; Kennedy 2006).

2.2 The Geostatistical Approach

Whereas standard GIS ignore statistical variation, geostatistics uses understanding of statistical variation as important source of information for improving prediction of an attribute at unsampled points, given a limited set of measurements (Burrough 2001). Geostatistical procedures, known as kriging, require an understanding of the principles of spatial statistic and provide statistically unbiased estimates of surface values from a set of control points. Kriging is a generic name, adopted by geostatisticians for a family of generalized least-squares regression algorithms (e.g., Stein 1999). The basic idea is to estimate the unknown attribute value at the unsampled location s_o as linear combination of neighbouring observations.

2.2.1 The Model for Ordinary Kriging and Cokriging

In ordinary kriging (OK) and cokriging (OCK), unbiased estimates of regionalized variables at unsampled point derive from the values of the surrounding stations using the spatial structural analysis and the initial set of measured data (Journel and Huijbregts 1978). Structural analysis (variography) assesses as to whether and to which extent an attribute is structured over the territory. The ability to identify the true spatial variability of a dataset depends, to a great extent, on ancillary knowledge of the underlying measured phenomenon (Diodato and Bellocchi 2008). Data may often be available for more than one attribute per sampled location. One set (Z) may be expensive to measure and therefore is seldom sampled while another (Y) may be cheap to measure and has more observations. If Z and Y are spatially correlated then it may be possible to use the information about the spatial variation of Y to help mapping Z. This can be done by using a multivariate extension of the normal kriging technique, known as cokriging (Burrough and McDonnell 1998).

In multivariate spatial modelling, semivariograms are used where the vertical axis represents one half of the squared difference between the values of paired locations, and the horizontal axis represents distance between locations. The experimental cross-covariance can be used to examine the local characteristics of spatial correlation (co-regionalization) between two datasets, and it can be used to look for spatial shifts in correlation between two datasets. Geostatistical Analyst module uses two stages for completing spatial modelling. Initially, an isotropic spherical model is assumed fitting the empirical semivariogram and cross-covariance function computed on the scaled data $\mathrm{Z}^\wedge{}_j^k(\mathbf{s}_i) = \mathrm{Z}_j^k(\mathbf{s}_i) \cdot \mathrm{s}_k^{-1}$, where $\mathrm{Z}_j^k(\mathbf{s}_i)$ is used to denote the j^{th} measurement of variable type k at the i^{th} spatial locations s_i, and s_k is the sample standard deviation. Then the standardized variables are unitless, they are standardised to unit variance and can be subtracted; incidentally they may have zero mean (important for analysis of the cross-variables) under symmetry assumptions (Cressie and Wikle 1998). Empirical semivariogram is called $\gamma_{\mathrm{ZZ}}(\mathbf{h})$ and cross-covariance $C_{\mathrm{ZY}}(\mathbf{h})$, where $_{\mathrm{Z}}$ indicates the precipitation variable and $_{\mathrm{Y}}$ indicates the elevation.

A kriged estimate of the variable at the location s_o is given by:

$$Z(s_o) = \lambda_z Z \quad \text{for ordinary kriging} \tag{1}$$

$$Z(s_o) = \lambda_z Z + \lambda_y Y \quad \text{for ordinary cokriging} \tag{2}$$

where $\mathbf{z}$ is a vector of the observed primary data (in our case they correspond to precipitation), $\mathbf{Y}$ is a vector of the observed secondary data (in our case they correspond to either elevation or topographic index) selected in the $\mathbf{s}_o$ neighbourhood observation $\mathbf{s}_j$, $\boldsymbol{\lambda}_z$ and $\boldsymbol{\lambda}_y$ are weight vector associated with the distance $h_{o(i)}$ (between $\mathbf{s}_o$ and $\mathbf{s}_i$) and $h_{o(j)}$ (between $\mathbf{s}_o$ and $\mathbf{s}_j$), respectively, and calculated by solving the kriging equation system (Johnston et al. 2001).

Geostatistical interpolation models can be evaluated by providing internal estimates of error. This was done by a reiterative process known as leave-one-out cross-validation. For each station we re-fitted the model leaving that station out of the data.

3 Results and Discussions

3.1 Terrain Conditioned–Precipitation

In meteorology and climatology, terrain characteristics are regarded as one of the main explanatory variables. However, in mountainous areas the stations are usually biased to the detriment of higher elevation on both local (Diodato and Ceccarelli 2005) and regional scales (Tveito 2007). This is particularly true for the Nepalese region, where rainfall and orographic variables differ significantly when the pattern is considered for each single sub-region moving from west to east (Fig. 3a–c).

Also in the same sub-region (ENH) under study, precipitation–DEM (P–DEM) relationships were not homogeneously distributed all over the study area (Fig. 3c). In this sub-region, exploratory data analysis applied to the original 59-sample precipitation datasets and supplied with the DEM co-variable, revealed a strong disproportionality towards higher elevations (Table 1).

This was so because ~78% of measurement stations are below 2,000 m, 12 stations (19%) between 2,000 and 4,000 m, and only two stations (3%) over 4,000 m. This is a strong drawback in a region where 60% of the land is located over 2,000 m. It should also be noted that due to complex rugged terrains, for atmospheric processes such as orographic channelling and convergence, simple negative/positive P–DEM correlations do not always hold. The general negative correlation between P and DEM was thus arranged at sub-regional scale (scatterplot of Fig. 3c). The optimal correlation elevation is not necessarily the point elevation, but more often is the effective elevation of a larger area (called the window) surrounding the observation point (Kyriakidis et al. 2001). For so, we decided to use DEM as covariate delineating it with 5×5 km^2 cells, in order to limit the contrast in elevation difference. Although these adjustments the new orographic surface remained affected by strong scale-large trend. As a consequence, in OCK processes the terrain surface was detrended prior to performing the structural geostatistical analysis. Slope and aspect variables were not included in the set of auxiliary variables because the intergauges distances were delineated at a greater scale than terrain-induced rainfall local transitions.

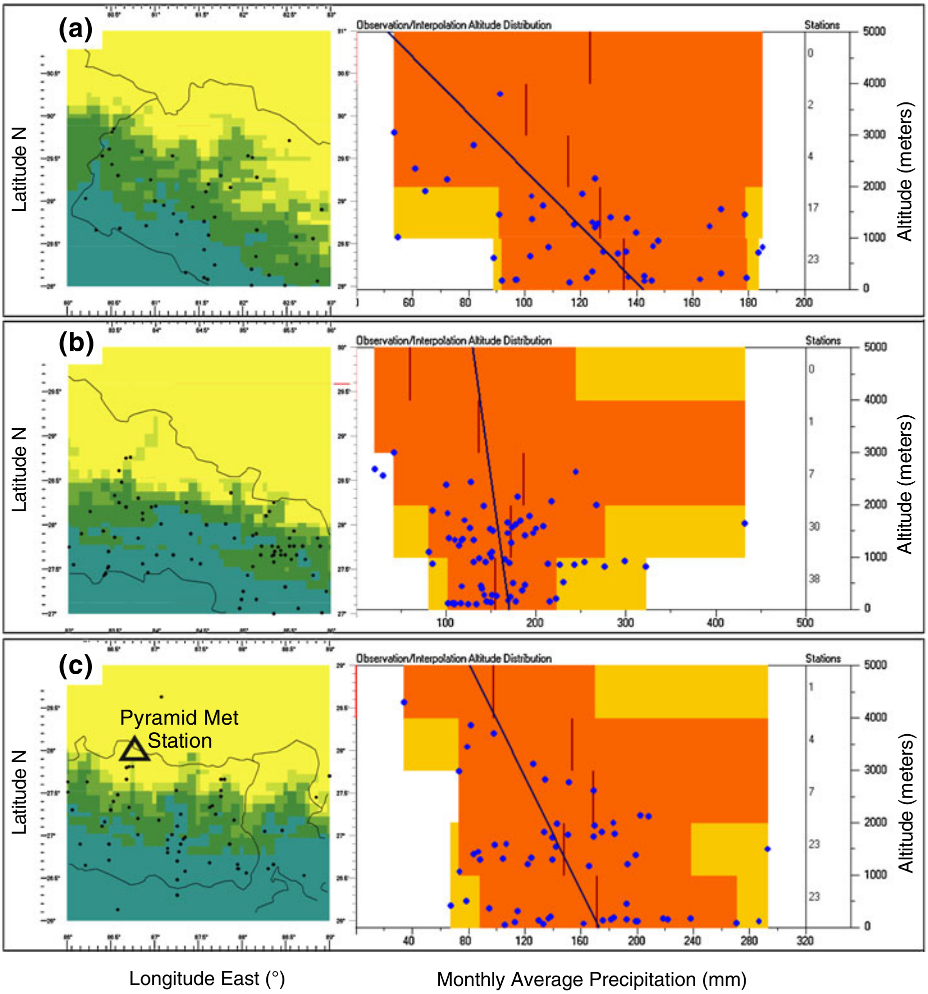

Fig. 3 Smoothed orography (5 × 5 km coloured cells) with increasing altitude from *green* to *yellow*, respectively, and with raingauges pattern (*black dots*) in single sub-area moving from west to east of the Nepal region [western (**a**), central (**b**) and eastern (**c**), respectively]; the correlation precipitation-elevation for each sub-region was also depicted in the respective scatterplots

However, the relationship between moisture flux direction and terrain aspect, the spatial gradient of moisture distribution, and terrain distance-influence were overall inferred through anisotropic and shifting cross-covariance functions.

3.2 Data Representativeness and Distribution

The resulting set of precipitation frequency distribution is reported in Fig. 4a–c, in which it is possible to note some little skewed distributions.

Table 1 Raingauge elevations and related annual precipitation descriptive statistics over 1961–1990 period in five sub-areas of Eastern Nepalese Highland

Sub-areas	Altitude range (m)	Area (km^2)	Stations number	5% rain percentile (mm)	Mean rain (mm)	95% rain percentile (mm)
5	>4,000	43,000	2 (3%)	216	1,200	1,908
4	3,000–4,000	4,560	4 (7%)	780	1,716	2,580
3	2,000–3,000	6,351	7 (12%)	1,092	1,944	2,760
2	1,000–2,000	10,986	22 (37%)	1,212	1,776	3,048
1	0–1,000	33,753	24 (41%)	1,224	2,112	3,204

Ordinary kriging (OK) and cokriging (OCK) are robust enough, and hold potential for applications even when the data do not have a robust normal distribution. The representativeness of the observational network is probably the most serious problem to deal with when spatializing environmental variables (Tveito 2007), strongly connected to covariate-conditioned climatological attributes. In our case, the general QQ-plot by plotting cumulative distributions data values for P–DEM introduces a dissimilarity in the joined distribution datasets, evidencing a biased distribution to the detriment of higher elevation and high hazard of performing partial extrapolation instead of complete interpolation (Fig. 5a–c).

3.3 Non-stationarity of the Data

Trend analysis showed the existence of a non-random (deterministic) component in spatial distribution of data over ENH: the largest gradient of the precipitation data occurs along the northwest to southeast direction. The partial south to north trend in precipitation can be attributed to persistent rainfall on the high mountains of pre-Himalayan chain. Nevertheless, we felt that the stationarity hypothesis does not hold for the whole region, but only locally. Strong non-stationarity was instead evident in elevation data. This may necessitate removing trend from these data, thus a local polynomial interpolation was chosen for it. The residual DEM-values were then used as input into the estimation of the residual semivariogram (i.e. the underlying trend-free semivariogram).

3.4 Multivariate Spatial Modelling

While performing multivariate spatial modelling, it was observed as the experimental semivariogram values increase with the separation distance, reflecting the assumption that rainfall data nearby tend to be more similar than rainfall data that

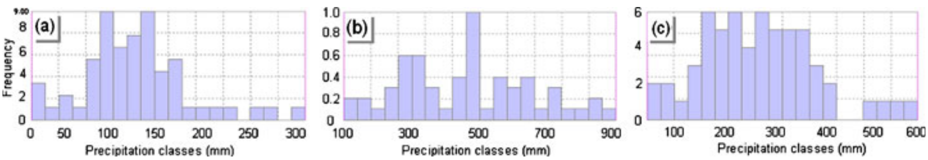

Fig. 4 Frequency distribution of precipitation in May (**a**), July (**b**) and September (**c**) from 59 sample stations data over eastern Nepal

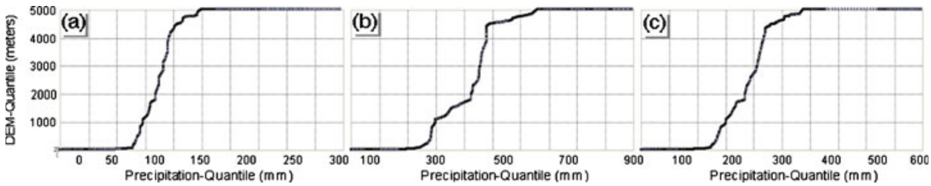

Fig. 5 General quantile-plots of precipitation–DEM cumulative distribution in May (**a**), July (**b**) and September (**c**) from 59 sample stations data over eastern Nepal

are farther apart. So parameters such as *range*, number of *lags* (assumed equal to seven), *nugget*, *partial sill*, *lag* size $\mathbf{h}$ (assumed equal to 0.1 decimal degrees $\approx$ 10 km $\approx$ minimum distance among the samples) and neighbourhood search size, included search data points. Directional influences were accounted for by calibrated interactively for performing spatial modelling. Also cross-covariances reflected the same assumption but with decreasing values, because the precipitation decreases with elevation at sub-region overall-scale but not at orographic meso-α down-scale.

The assumption of an isotropic model was not verified, thus the semivariograms and cross-covariance functions were modelled on directional components (anisotropy) within a combination of two distinct spatial structures: *nugget variance* and *Hole effect*, for May, and *nugget variance* and *Spherical structure*, for July and September. However, during the manipulation stage, the performance was attained by coupling anisotropy and shift effects in May, July and September months. This can be explained because of very steeply slopes and windy tracking pre-Himalayan chain, so that the time lag between the condensation phenomenon and acceleration of the moist air mass can move in that downwind direction (e.g., interposed valley between two or more mountains) the maximum value of the precipitation.

Also anisotropy is a characteristic of a random process common to all the monsoon rainy seasons which show higher autocorrelation in one direction than another varying mainly with wind direction. This can be attributed to pre-Himalayan orographic barriers branching out toward WestNorthWest–EastSouthEast and North–South. For this reason, when the empirical semivariograms and cross-covariances for the raingauge-points are plotted, the spatial relationship is different in each direction: in the North–South direction, the shape of the model curves increases more rapidly before levelling out, for May, and in WestNorthWest–EastSouthEast, for July and September months.

Regarding the model structures, the spherical (Sph)-function is the most widely used semivariogram, characterized by linear behaviour at the origin, which fits well in July and September months, when airflows easily penetrate in the valley towards South to North and successively ramifying towards WestNorthWest or EastNorthEast. The *Hole effect* (HE)-function typically reflects cyclic phenomena (Journel and Huijbregts 1978), which fit well in May, when the wind coming still from West is forced to pass over to follow one to another mountainous chain. In this way, accounting for direction-dependent variability (geometric anisotropy) and spatial pattern-shift effects, the $\gamma(h, \theta)$ and $C(h, \theta)$ models were explained for the following months:

$$\textbf{May}\begin{cases} \gamma_{ZZ}(h,\theta) = 480_{\text{(Nugget)}} & |\mathrm{h}| = 0 \\ \gamma_{ZZ}(h,\theta) = 480_{\text{(Nugget)}} + 1717_{\text{(Partial·Sill)}} \cdot \text{HoleEffect}(|\mathrm{h}|, \Omega(\theta)) & |\mathrm{h}| > \Omega(\theta) \\ \gamma_{YY}(h,\theta) = 41323_{\text{(Nugget)}} & |\mathrm{h}| = 0 \\ \gamma_{YY}(h,\theta) = 41323_{\text{(Nugget)}} + 168749_{\text{(Partial·Sill)}} \cdot \text{HoleEffect}(|\mathrm{h}|, \Omega(\theta)) & |\mathrm{h}| > \Omega(\theta) \\ C_{ZY}(h,\theta) = -12847_{\text{(PartialSill)}} & |\mathrm{h}| = 0 \\ C_{ZY}(h,\theta) = -12847 \cdot \text{HoleEffect}(|\mathrm{h}|, \Omega(\theta))_{shift} & |\mathrm{h}| > \Omega(\theta) \end{cases} \tag{3}$$

where Ω defines the anisotropy, θ is the direction of the lag, and $_{\text{shift}}$ defines the asymmetry of the cross-covariance function; the *Hole effect* functions are equal to:

$$\left\{\frac{1-\sin\left(\frac{2\Pi|\mathrm{h}|}{\Omega(\theta)}\right)}{\sin\left(\frac{2\Pi|\mathrm{h}|}{\Omega(\theta)}\right)}\right\}, \text{ for } \gamma(h,\theta), \text{ and}: \left\{\frac{1+\sin\left(\frac{2\Pi|\mathrm{h}|}{\Omega(\theta)}\right)}{\sin\left(\frac{2\Pi|\mathrm{h}|}{\Omega(\theta)}\right)}\right\}, \text{ for } C(h,\theta);$$

$$\textbf{July}\begin{cases} \gamma_{ZZ}(h,\theta) = 3000_{\text{(Nugget)}} & |\mathrm{h}| = 0 \\ \gamma_{ZZ}(h,\theta) = 3000_{\text{(Nugget)}} + 35000_{\text{(Partial·Sill)}} \cdot \text{Sph}(|\mathrm{h}|, \Omega(\theta)) & 0 < |\mathrm{h}| \le \Omega(\theta) \\ \gamma_{ZZ}(h,\theta) = 35000_{\text{(Partial·Sill)}} & |\mathrm{h}| > \Omega(\theta) \\ \gamma_{YY}(h,\theta) = 0_{\text{(Nugget)}} & |\mathrm{h}| = 0 \\ \gamma_{YY}(h,\theta) = 0_{\text{(Nugget)}} + 210830_{\text{(Partial·Sill)}} \cdot \text{Sph}(|\mathrm{h}|, \Omega(\theta)) & 0 < |\mathrm{h}| \le \Omega(\theta) \\ \gamma_{ZZ}(h,\theta) = 210830_{\text{(Partial·Sill)}} & |\mathrm{h}| > \Omega(\theta) \\ C_{ZY}(h,\theta) = -78262 \cdot \text{Sph}(|\mathrm{h}|, \Omega(\theta))_{shift} & 0 < |\mathrm{h}| \le \Omega(\theta) \\ C_{ZY}(h,\theta) = -78262_{\text{(Partial·Sill)}} & |\mathrm{h}| > \Omega(\theta) \end{cases} \tag{4}$$

$$\textbf{Sept}\begin{cases} \gamma_{ZZ}(h,\theta) = 1266_{\text{(Nugget)}} & |\mathrm{h}| = 0 \\ \gamma_{ZZ}(h,\theta) = 1266_{\text{(Nugget)}} + 12055_{\text{(Partial·Sill)}} \cdot \text{Sph}(|\mathrm{h}|, \Omega(\theta)) & 0 < |\mathrm{h}| \le \Omega(\theta) \\ \gamma_{ZZ}(h,\theta) = 12055_{\text{(Partial·Sill)}} & |\mathrm{h}| > \Omega(\theta) \\ \gamma_{YY}(h,\theta) = 0_{\text{(Nugget)}} & \mathrm{h} = 0 \\ \gamma_{YY}(h,\theta) = 0_{\text{(Nugget)}} + 213962_{\text{(Partial·Sill)}} \cdot \text{Sph}(|\mathrm{h}|, \Omega(\theta)) & 0 < |\mathrm{h}| \le \Omega(\theta) \\ \gamma_{ZZ}(h,\theta) = 213962_{\text{(Partial·Sill)}} & |\mathrm{h}| > \Omega(\theta) \\ C_{ZY}(h,\theta) = -50787 \cdot \text{Sph}(|\mathrm{h}|, \Omega(\theta))_{shift} & 0 < |\mathrm{h}| \le \Omega(\theta) \\ C_{ZY}(h,\theta) = -50787_{\text{(Partial·Sill)}} & |\mathrm{h}| > \Omega(\theta) \end{cases} \tag{5}$$

where the *Spherical* functions are equal to: $\left\{\frac{3\cdot|\mathrm{h}|}{2\cdot\Omega(\theta)} - \frac{1}{2}\left(\frac{|\mathrm{h}|}{\Omega(\theta)}\right)^3\right\}$, for $\gamma(h, \theta)$, and: $\left\{1 - \frac{3\cdot|\mathrm{h}|}{2\cdot\Omega(\theta)} + \frac{1}{2}\left(\frac{|\mathrm{h}|}{\Omega(\theta)}\right)^3\right\}$, for $C(h, \theta)$.

The function that defines the anisotropy is $\Omega(\theta) = [a^2\cos^2(\theta - \varphi) + b^2\sin^2(\theta-\varphi)]^{0.5}$, where a and b are the maximum (major *range*) and minimum (minor *range*) diameters of elliptic model shape, respectively.

The model shape and neighbourhood search size are strongly connected, so it is important to define also the neighbourhood type and the constraints of the points within the neighbourhood that will be used in the prediction of an unsampled location. Of course, the choice of the neighbourhood reflects the shape and bands of precipitation, taking anisotropic forms over these complex terrains. Regarding to shape of the cross-covariance, the neighbourhood results also asymmetric, because the performing process shows that $Z(\mathbf{s}_i)$ and $Y(\mathbf{s}_j)$ have not the highest cross-covariance when $\mathbf{s}_i = \mathbf{s}_j$, and the cross-covariance decreases differently as $\mathbf{s}_i$ and $\mathbf{s}_j$ get farther apart. So, the cross-covariance results are "shifted" over all the months, i.e. $C(\mathbf{s}_i,\mathbf{s}_j) \neq C(\mathbf{s}_i,\mathbf{s}_j)$.

3.5 Precipitation Climate Spatial Patterns

Figure 6 shows the final spatial patterns of cokriging estimates and related error maps of average monthly precipitation of May, July and September on a 4 by 4 km grid-resolution over ENH. According to *Hole Effect* model, precipitation in May (Fig. 6a_1) implies that the short-range variations of rain are regularly affected by local topographic characteristics, although the spatial pluviometric range is moderate (0–300 mm). The successive months see heavy Indian summer monsoon providing a considerable rain amount at southern plains extending from east to west with 800–500 mm in July, and 600–200 mm in September (Fig. 6b_1 and c_1, respectively).

By moving from the foot of the Plateau, rainy bands along south-eastern flanks of the slopes become intense but more discontinuous, crowning the mountainous bulwark around the Sagarmatha National Park where 900 mm are reached in July and 600 mm in September (Fig. 6b_1 and c_1, respectively). This is caused by the horizontal extension of hill and mountain ranges (orographic *Hole effect*), resulting with moist conditions on South and East facing slopes with major rain shadow on the northern sides of the slopes. August (map not shown) and September present similar characteristics to July, but with lower rain totals, especially in September (Fig. 6c_1).

The direct effects of elevation do not appear to affect precipitation below scales of about 5–10 km. However, this represents a hidden rain field that is caused mainly by variability of data that cannot be detected at the scale smaller of sampling (<5–10 km). At this micro-local scale, hydrometeor trajectories simulations give rise to some interesting possibilities such as: a precipitation rate that maximizes at intermediate values of the horizontal wind speed, localized precipitation efficiencies in excess of 100%, and a reverse rain shadow with more precipitation falling on the leeward flank than on the windward flank (Roe and Baker 2006).

In order to give also an idea of interpolation spatial errors, in Fig. 6a_2, b_2, c_2 are depicted kriging error maps that present all little values around 100 mm month^{-1}. Only in July, kriging errors reach values around 200 mm month^{-1} at North and, marginally, at South of the area. However, orography of both these areas is prevalently flat and therefore the actual error values can be considered lower than 200 mm.

Finally, we inspected vertical precipitation at orographic meso-α spatial scale (~30 km), within an atmospheric circulation in the 90° East latitude–altitude cross-section for July month (Fig. 7). From this scheme it is possible to argue that the rainfall variation derived from cokriged-map of Fig. 6b, according to profile-pattern of the relative humidity (purple bands draping the terrain profile). It is in fact evident that the mountains pre-Tibetan Plateau (placed below the 28th parallel North, Fig. 7 latitudinal-axis) triggers an orographic forcing for intensifying precipitation processes which turn off with the altitude when moving northward to the Plateau.

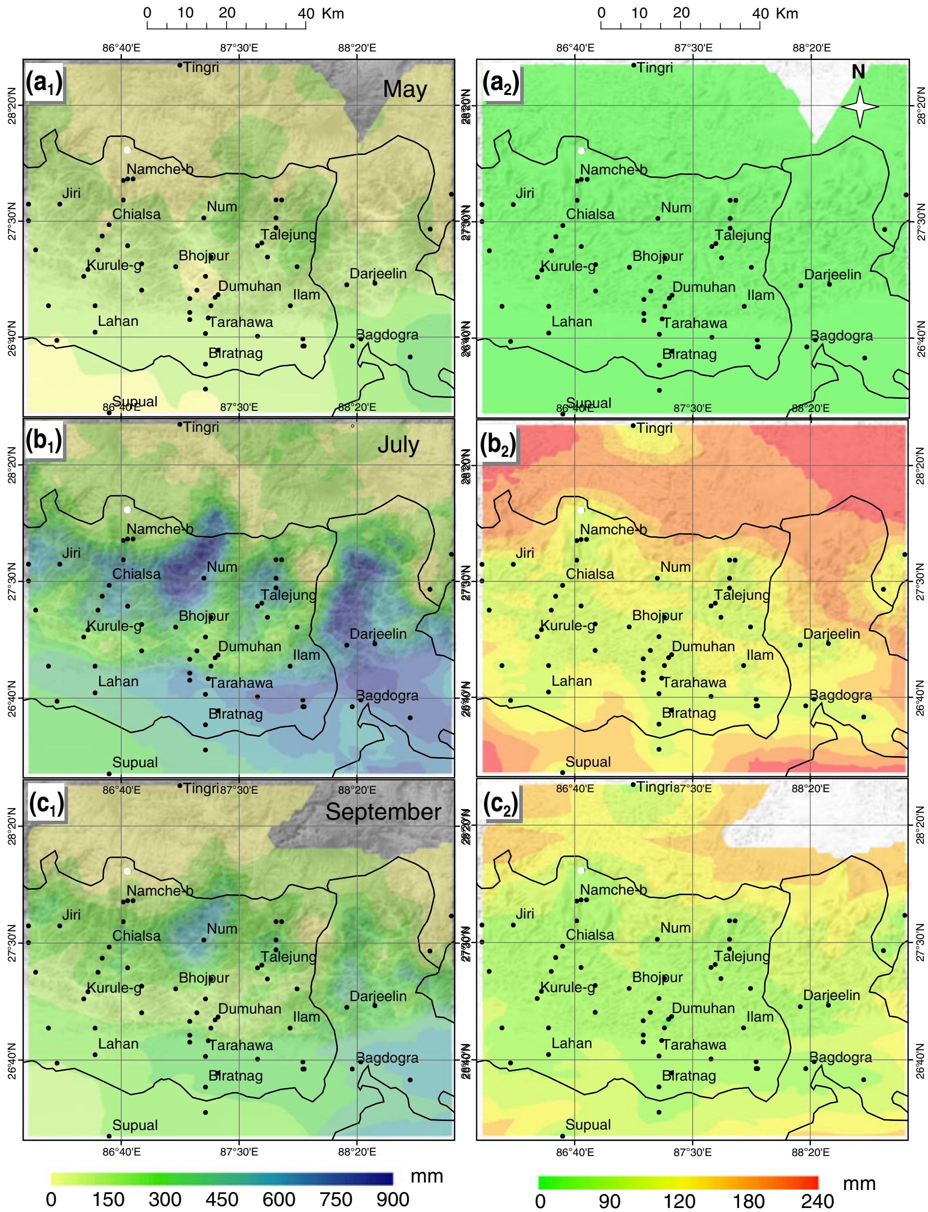

Fig. 6 Cokriged maps of average monthly precipitation (in mm) over eastern Nepal for May (a_1), July (b_1) and September (c_1) superimposed to orographic hillshade, and respective cokriged errors maps in May (a_2), July (b_2) and September (c_2). *White circle* close Namche-h location indicates the AWS Pyramid

Rain increase positively follows the air moisture (purple bands magnitude along ramped slope between 27 and 28° N, where precipitation is around 600 mm), then rain gradually decreases around 28° N, when the terrain reaches the maximum

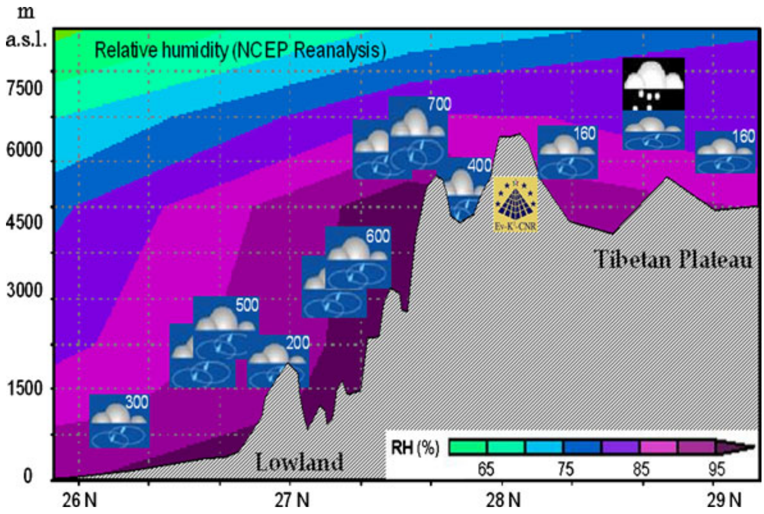

Fig. 7 Terrain transect South–North with relative humidity profile (coloured bands from *green* to *purple*) in the altitude–latitude section crossing AWS Pyramid and *rain-symbols* indicating monthly precipitation quantities (in the corner of any *rain-symbol*) based on July cokriged-climate-map of **b** (humidity profile by NCEP-reanalysis, http://www.cdc.noaa.gov)

altitude (above m 6,000 a.s.l.) after a valley, and continues to decline until the AWS Pyramid. Minimum of rain total in July is reached above the Tibetan Plateau where precipitable water is scarce because the smallest thickness of air-humidity on this place compared to adjacent slope and lowlands.

It is also worth-noting that the stronger increase in rain does not originate from the southern pre-Tibetan mountains, but is originated at the southern edge near the foot, when rainfall amount in July suddenly passes from 200 to 600 mm, according to strong upward motion of air (up to 20 hPa h^{-1}, Chow and Chan 2009) in the southern flank of the Tibetan Plateau.

3.6 Assessing Models Performance

The results of the cross-validation process are shown in the scatterplots of Fig. 8. From these graphs it is possible to detect good agreement between modelled and observed monthly precipitation for May (8a), July (8b) and September (8c) by cokriging.

The disadvantage of cross-validation is that no error information is provided for places where there are no stations (Daly 2006). To overcome such drawback the climate dataset may be independently evaluated by assessing its consistency with other spatial attributes (e.g., Milewska et al. 2005). For this, vegetation greenness pattern and precipitation were considered for July, for assessing their spatial consistency over an area surrounding the Sagarmatha National Park (Northeastern of the sub-region under study in Fig. 9). This assumption was supported by the strong correspondence found by Ding et al. (2007), between annual maximum Normalized

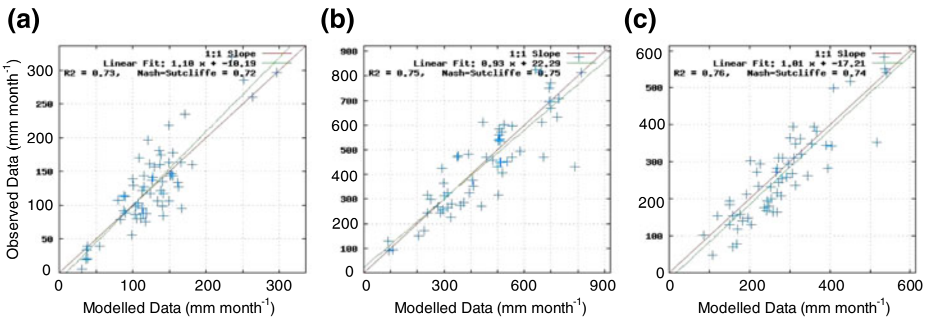

Fig. 8 Scatterplots between modelled and observed monthly precipitation for May (**a**), July (**b**) and September (**c**) by ordinary cokriging cross-validation

Differential Vegetation Index (NDVI) and annual effective precipitation in most parts of southern Tibet, southern slope of Himalaya and grassland of these regions.

In our case cokriging yielded a visible and large consistency with the NDVI map, whereas kriging confirmed lack of accuracy to reproduce the vegetation pattern. The goof performance of cokriging is remarkable, in an area where intergauge distances were delineated at a greater scale than the DEM-orographic scale. This result supports the use of multivariate geostatistical models as flexible approaches for estimating precipitation spatial pattern in remote areas.

4 Concluding Remarks

The results of this study indicate that the use of the multivariate geostatistical model would be suitable for predicting precipitation patterns in the eastern Nepalese region. Considerable spatial variations in precipitation were observed, due to the exceptionally rugged terrain of this area. Moreover, the primary sampled data

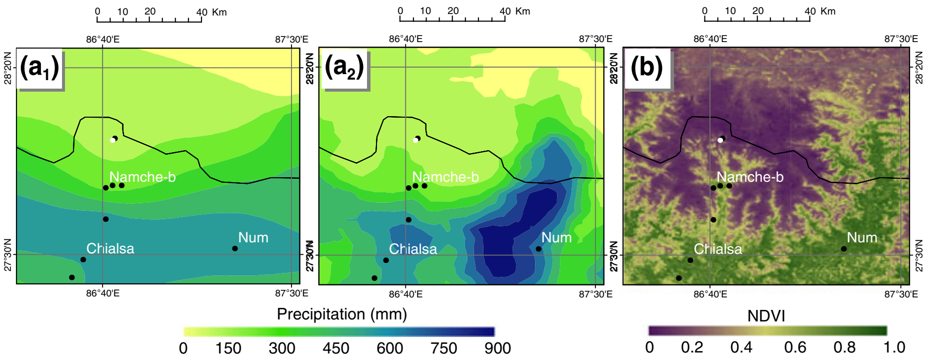

Fig. 9 Kriged (a_1) and cokriged (a_2) precipitation maps for July compared to NDVI pattern (b) around the Sagarmatha National Park (at Northwestern of the Nepal sub-area under study)

often presented an irregular spatial pattern (e.g., clustered data, sparse data, under-representativeness of the primary data in comparison to auxiliary data), making modelling precipitation some more complicate for the purpose of statistical inference over ungauged areas in the region. The minimum density of rain-gauges recommended by the World Meteorological Organization (http://www.wmo.int) for pluviometric networks calls for more stations (i.e., about 200 to 500 raingauges over eastern Nepal) than those available and here used (59 stations with records included in the period 1961–1990). Whether more efforts are needed to further reduce the observational biases and other uncertainties in precipitation estimates, the cokriging approach (multivariate geostatistical mapping) resulted in the production of reasonably accurate finer resolution (downscaling) maps (for the monsoonal months of May, July and September) covering the same spatial extent. Improved regional precipitation climatology was derived and the results of this study will be useful to hydrological and climatic studies in the high elevation Himalayan areas.

This study also raised the need of both spatial and temporal assessments over a landscape as rugged as the Nepalese region. The analysis conducted was a static vision of precipitation patterns, while climate is constantly changing from year to year as well as from decade to decade. For instance, an analysis of the frequency of extreme precipitations, with rainfall exceeding 100 mm within 24 h, occurring between 1971 and 1990 over Nepal region, indicated an increasing trend of such events (Chalise and Khanal 2001). Also in a more recent analysis (Sheikh et al. 2005), extended up to year 2000, extreme indices indicated an increasing tendency of precipitations in Nepal. This clearly calls for further studies for expanding the path tracked by this study.

Acknowledgements This research is a contribution to a wider project (CEOP-High Elevations; http://www.ceop-he.org) to assess hydroclimatological and water resource patterns in high altitude areas of the world. It is a concerted, international and interdisciplinary effort aimed to advance knowledge on physical and dynamical processes at high altitude areas.

References

Anders AM, Roe GH, Hallet B, Montgomery DR, Finnegan NJ, Putkonen J (2006) Spatial patterns of precipitation and topography in the Himalaya. In: Willett SD, Hovius N, Brandon MT, Fisher D (eds) Tectonics, climate, and landscape evolution. Geological Society of America, Special Paper 398. Geological Society of America, Boulder, pp 39–53

Arora M, Singh P, Goel NK, Singh RD (2006) Spatial distribution and seasonal variability of rainfall in a mountainous basin in the Himalayan region. Water Resour Manag 20:489–508

Aspinall R, Pearson D (2000) Integrated geographical assessment of environmental condition in water catchment: linking landscape ecology, environmental modelling and GIS. J Environ Manag 59:299–319

Attorre F, Alfò M, De Sanctis M, Francesconi F, Bruno F (2007) Comparison of interpolation methods for mapping climatic and bioclimatic variables at regional scale. Int J Climatol 27:1825–1843

Barros AP, Lang TJ (2003) Monitoring the monsoon in the Himalayas: observations in central Nepal. Mon Weather Rev 131:1408–1427

Basistha A, Arya DS, Goel NK (2008) Spatial distribution of rainfall in Indian Himalayas—a case study of Uttarakhand Region. Water Resour Manag 22:1325–1346

Bertolani L, Bollasina M, Verza GP, Tartari G (2000) Pyramid meteorological station Sagarmatha national park 5050 m—Lobuche, Khumbu Valley, Nepal. Summary Report 1994–1998, Ev-K^2-CNR Committee, Milan

Bhowmik SKR, Das AK (2007) Rainfall analysis for Indian monsoon region using the merged rain gauge observations and satellite estimates: evaluation of monsoon rainfall features. J Earth Syst Sci 116:187–198
Bindlish R, Barros AP (2000) Disaggregation of rainfall for one-way coupling of atmospheric and hydrologic models in regions of complex terrain. Glob Planet Change 25:111–132
Bookhagen B, Burbank DW (2006) Topography, relief, and TRMM-derived rainfall variations along the Himalaya. Geophys Res Lett 33:L08405. doi:10.1029/2006GL026037
Burrough PA (2001) GIS and geostatistics: essential partners for spatial analysis. Environ Ecol Stat 8:361–377
Burrough PA, McDonnell RA (1998) Principles of geographical information systems. Oxford University Press, Oxford
Chalise SR, Khanal NR (2001) Rainfall and related natural disasters in Nepal. In: Li T, Chalise SR, Upreti BN (eds) Landslide hazard mitigation in the Hindu Kush-Himalayas. ICIMOD, Kathmandu, pp 63–70
Chow KC, Chan JCL (2009) Diurnal variations of circulation and precipitation in the vicinity of the Tibetan Plateau in early summer. Clim Dyn 32:55–73
Cressie N, Wikle CK (1998) The variance-based cross-variogram: you can add apples and oranges. Math Geol 30:789–799
Dahal KR, Hasegawa S, Masuda T, Yamanaka M (2006) Roadside slope failures in Nepal during torrential rainfall and their mitigation. In: Marui H, Marutani T, Watanabe N, Kawabe H, Gonda Y, Kimura M, Ochiai H, Ogawa K, Fiebiger G, Heumader J, Rudolf-Miklau F, Kienholz H, Mikos M (eds) Distaster mitigation of debris flows, slope failures and landslides. Universal Academy, Tokyo, pp 503–514
Daly C (2006) Guidelines for assessing the suitability of spatial climate data sets. Int J Climatol 26:707–721
Daly C, Neilson RP, Phillips DL (1994) A statistical–topographic model for mapping climatological precipitation over mountainous terrain. J Appl Meteorol 33:140–158
Daly C, Gibson WP, Taylor GH, Johnson GL, Pasteris P (2002) A knowledge-based approach to the statistical mapping of climate. Clim Res 22:99–113
Dhar ON, Nandargi S (2005) Areas of heavy precipitation in the Nepalese Himalayas. Weather 60:354–356
Ding M, Zhang Y, Liu L, Zhang W, Wang Z, Bai W (2007) The relationship between NDVI and precipitation on the Tibet Plateau. J Geogr Sci 17:259–268. doi:10.1007/s11442-007-0259-7
Diodato N (2005) The influence of topographic co-variables on the spatial variability of precipitation over small regions of complex terrain. Int J Climatol 25:351–363
Diodato N, Bellocchi G (2008) Drought stress patterns in Italy using agro-climatic indicators. Clim Res 36:53–63
Diodato N, Ceccarelli M (2005) Processes using multivariate geostatistics for mapping interpolation of climatological precipitation mean in the Sannio Mountains (southern Italy). Earth Surf Process Landf 30:259–268
Goovaerts P (2000) Geostatistical approaches for incorporating elevation into the spatial interpolation of rainfall. J Hydrol 228:113–129
Grieser J, Gommes R, Bernardi M (2006) New LocClim—the local climate estimator of FAO. Geophys Res Abstr 8:SRef-ID:1607–7962/gra/EGU06-A-08305
Jain SK, Kumar S, Varghese J (2001) Estimation of soil erosion for a Himalayan watershed using GIS technique. Water Resour Manag 15:41–54
Johnston K, ver Hoef JM, Krivoruchko K, Lucas N (2001) Using ArcGIS geostatistical analyst. ESRI, Redlands
Journel AG, Huijbregts CJ (1978) Mining geostatistics. Academic, London
Kansakar SR, Hannah DM, Gerrard J, Rees G (2004) Spatial pattern in the precipitation regime of Nepal. Int J Climatol 24:1645–1659
Kennedy M (2006) Introducing geographic information system with ArcGIS: featuring GIS software from Environmental Systems Research Institute. Wiley, Hoboken
Kyriakidis PC, Kim J, Miller NL (2001) Geostatistical mapping of precipitation from rain gauge data using atmospheric and terrain characteristics. J Appl Meteorol 40:1855–1877
Lang TJ, Barros AP (2004) Winter storms in the central Himalayas. J Japan Meteorol Soc 82:829–844
Leemans R, Cramer W (1991) The IIASA database for mean monthly values of temperature, precipitation and cloudiness of a global terrestrial grid. RR-91-18. International Institute for Applied Systems Analysis (IIASA), Laxenburg

Milewska EJ, Hopkinson RF, Niitsoo A (2005) Evaluation of geo-referenced grids of 1961–1990 Canadian temperature and precipitation normals. Atmos Ocean 43:49–75
Mirás-Avalos JM, Mestas-Valero RM, Sande-Fouza P, Paz-González A (2009) Consistency analysis of pluviometric information in Galicia (NW Spain). Atmos Res 94:629–640
Pons X, Ninyerola M (2008) Mapping a topographic global solar radiation model implemented in a GIS and refined with ground data. Int J Climatol 28:1821–1834
Roe GH, Baker MB (2006) Microphysical and geometrical controls on the pattern of orographic precipitation. J Atmos Sci 63:61–880
Sharma CK (1979) Partial drought conditions in Nepal. Hydrol Sci Bull 24:327–333
Sheikh MM, Ahmed AU, Kolli RK, Shrestha ML, Dharmaratna GHP (2005) Development and application of climate extreme indices and indicators for monitoring trends in climate extremes and their socio-economic impacts in South Asian countries. Final report for Asia-Pacific Network project 2005-10-NSY-Sheikh, Islamabad
Shrestha ML (2000) Inter annual variation of summer monsoon rainfall over Nepal and its relation to Southern Oscillation Index. J Meteorol Atmos Phys 75:21–28
Singh P (1997) Effect of orography on precipitation in the western Himalayan region. J Hydrol 199:183–206
Singh KK, Singh SV (1996) Space–time variation and regionalization of seasonal and monthly summer monsoon rainfall of the sub-Himalayan region and Gangetic plains of India. Clim Res 6:251–262
Smith RB (1979) The influence of mountains on the atmosphere. Adv Geophys 21:87–230
Stein ML (1999) Statistical interpolation of spatial data: some theory for Kriging. Springer, New York
Tveito OE (2007) The developments in spatialization of meteorological and climatological elements. In: Dobesch H, Dumolard P, Dyras I (eds) Spatial interpolation for climate data. ISTE, Newport Beach, pp 73–86
Vicente-Serrano SM, Lanjeri S, López-Moreno JI (2007) Comparison of different procedures to map reference evapotranspiration using geographical information systems and regression-based techniques. Int J Climatol 27:1103–1118
Yatagai A, Kawamoto H (2008) Quantitative estimation of orographic precipitation over the Himalayas by using TRMM/PR and a dense network of rain gauges. Proc SPIE 7148-11. doi:10.1117/12.811943
Yatagai A, Xie P, Kitoh A (2005) Utilization of a new gauge-based daily precipitation dataset over monsoon Asia for validation of the daily precipitation climatology simulated by the MRI/JMA 20-km-mesh AGCM. SOLA 1:193–196. doi:10.2151/sola.2005-050
Yin Z-Y, Zhang X, Liu X, Colella M, Chen X (2008) An Assessment of the biases of satellite rainfall estimates over the Tibetan Plateau and correction methods based on topographic analysis. J Hydrometeorol 9:301–326
Zhou S, Xue G, Gong P, Chen J, Zhang H, Zhou Z, Fan X, Deng X, Zhanping WU (2005) The SIA method for spatial analysis of precipitation in the upper-middle reaches of the Yangtze River. J Geogr Sci 15:223–238